Research Article | Vol. 11, No. 8 / 1 August 2021 / Optical Materials Express 2528

Optical Materials EXPRESS

Visible to near-infrared broadband fluorescence from Ce-doped silica fiber

AMIT YADAV,[1,*] NIKOLAI B. CHICHKOV,[1] REGINA GUMENYUK,[2] HARRI ALI-LÖYTTY,[2] KIMMO LAHTONEN,[2] MIKA VALDEN,[2] MIKHAIL A. MELKUMOV,[3] MIKHAIL V. YASHKOV,[4] EVGENY ZHEREBTSOV,[5] AND EDIK U. RAFAILOV[1]

[1]*Aston Institute of Photonic Technologies, Aston University, B4 7ET, Birmingham, UK*
[2]*Laboratory of Photonics, Tampere University of Technology, Tampere, Finland*
[3]*Prokhorov General Physic Institute of the Russian Academy of Sciences, Dianov Fiber Optics Research Center, Moscow 119333, Russia*
[4]*Devyatykh Institute of Chemistry of High-Purity Substances of the Russian Academy of Sciences, Nizhny Novgorod 603600, Russia*
[5]*Optoelectronics and Measurement Techniques, University of Oulu, Oulu, FI - 90014, Finland*
[*]*a.yadav1@aston.ac.uk*

Abstract: We investigate the fluorescence characteristics of a purely Ce-doped silica fiber and demonstrate broad-bandwidth fluorescence across the visible and near-infrared. The Ce-doped fiber is fabricated using standard modified chemical vapor deposition technology. Trace metal analysis by inductively coupled plasma mass spectrometry confirmed the purity of Ce-doping. The Ce valence state of 3+ was revealed by X-ray photoelectron spectroscopy. The optimum pump wavelength for the broadest luminescence from a fiber is scanned between 405 nm to 440 nm wavelength of diode lasers operating under continuous-wave regime. The strongest pump absorption is observed at the wavelength of 405 nm. Variation of pump power and fiber length results in the demonstration of broad-bandwidth fluorescence with spectral widths up to 301 nm (at -10 dB). The measured fluorescence spectra cover the wavelength range from ~458 nm to ~819 nm with spectral power densities of up to 2.4 nW/nm.

1. Introduction

Ce-ions have been investigated as independent luminescence centers and sensitizers in a wide range of materials [1–3]. Ce-doping and $Ce^{3+}Ln^{3+}$ -codoping have been demonstrated in different host materials including crystals, silicate, aluminosilicate, phosphate, fluoride glasses and fibers [4–10]. Generally, the 5d-4f transition in Ce-ions results in broadband fluorescence across the visible wavelength region of 450-550 nm under UV excitation. However, an emission band can be shifted towards longer wavelengths in the presence of high crystal field as it was demonstrated for Ce-doped garnets and ceramics [11,12]. The potential emission in blue-green-yellow wavelength range makes these materials highly interesting for applications as scintillators [13,14] and white light emitters [15]. Ce-doped fibers provide high spectral power densities and fluorescence across the entire visible part of the optical spectrum [8,16]. Therefore, they are of great interest as light sources for high resolution optical coherence tomography (OCT) [16,17]. Additionally, Ce-doped fibers are promising candidates for the realization of visible light emitters and for applications in visible light communication. Towards this, the primary requirements for such fibers would be to use non-UV pump sources and provide broadband emission across the visible part of the optical spectrum from a single fiber.

#432560 https://doi.org/10.1364/OME.432560
Journal © 2021 Received 26 May 2021; revised 30 Jun 2021; accepted 4 Jul 2021; published 14 Jul 2021

Optical Materials EXPRESS

In this paper, we investigate the fluorescence properties of a novel pure Ce-doped silica fiber. The fiber is prepared using modified chemical vapor deposition (MCVD) technique. We perform trace metal analysis as well as an identification of valence states of cerium ions. The fluorescence spectra are examined at different pump wavelengths between 405 nm and 440 nm including these two wavelengths. The influence of fiber lengths and pump power on the obtained fluorescence spectra is analyzed. By optimization of fiber length and pump power, we demonstrate broadband fluorescence with a spectral width of 301 nm (at -10 dB). To the best of our knowledge, this is the broadest fluorescence bandwidth that has been obtained from Ce-doped fibers spanning across the visible and the NIR part of the optical spectrum. Such broad luminescence from a single fiber might be a robust solution for many applications in bioimaging.

2. Experimental details

2.1. Fabrication of Ce-doped fiber

The Ce-doped silica fiber is drawn from a preform fabricated by standard MCVD technology, supplemented by the impregnation method. The technological process of fabricated preform consists of several stages. At the first stage, a reflecting cladding made of F-SiO_2 composition with $\Delta n \sim$ -0.005 is deposited. $SiCl_4$ and SiF_4 are used as precursors (see Fig. 1(top)). Then a second layer is deposited in the form of "soot" , containing only SiO_2. This "soot" layer is impregnated with a water-alcohol solution of Ce $(NO_3)_3$. After that, the porous layer is dried and then vitrified into a transparent glass. Finally, the tube is collapsed and sealed [18]. The fiber sample was drawn on the drawing tower with the geometrical parameters of ~13 μm core and ~146 μm cladding diameters. The refractive index profile of the fiber is similar to the refractive index profile of the preform (see Fig. 1(top)).

2.2. Characterization of Ce-doped fiber

Absorption spectrum of the Ce-doped fiber was measured using several light sources in the wavelength range of 400 nm to 1700 nm using a cut-back method. For an excitation wavelength around 400 nm an absorption of 200 dB/m is observed for the fiber (see Fig. 1(bottom)).

Next, we performed trace metal analysis of the Ce-doped glass fiber with respect to rear-earth (RE) elements (Ce, Pr, Nd, Sm, Eu, Gd, Tb, Dy, Ho, Er, Tm, Yb, Lu) by inductively coupled plasma mass spectrometry (ICP-MS) method using Thermo Scientific iCAP RQ equipment. For the ICP-MS measurement a piece of glass fiber was acid digested (see Appendix A for further details on the experiment) and the results shown in Table 1 are normalized to the fiber mass. The analysis indicated that there were no other active RE ions except Ce. Therefore, our glass samples are purely Ce-doped, and all luminescence is taking place via energy transfer between energy levels of Ce ions exclusively.

Table 1. ICP-MS - Trace metal analysis of rear-earth elements in the Ce-doped glass fiber. The concentration of RE elements other than Ce were below the detection limit (d.l.).

ppm	Ce	Pr	Nd	Sm	Eu	Gd	Tb	Dy	Ho	Er	Tm	Yb	Lu
d.l.	0.05	0.02	0.07	0.03	0.07	0.02	0.01	0.01	0.02	0.01	0.01	0.02	0.02
Ce-doped glass fiber	29.67	<d.l.	<d.l.	<d.l.	<d.l.	<d.l.	<d.l.	<d.l.	<d.l.	<d.l.	<d.l.	<d.l.	<d.l.

It is well known that Ce ion usually appears in trivalent oxidation state in the glass matrix as this is energetically most favorable state [11,12]. However, quite often, under certain conditions, polyvalent cerium ion (Ce^{3+} and Ce^{4+}) may also form to attain internal equilibrium. Their ratio depends on various parameters including melting temperature, glass composition and the oxygen activity of the melt [6]. In light of these facts we used X-ray photoelectron spectroscopy (XPS) to analyze Ce-ion valency in the glass sample as shown in Fig. 2. XPS was performed by employing

Optical Materials EXPRESS

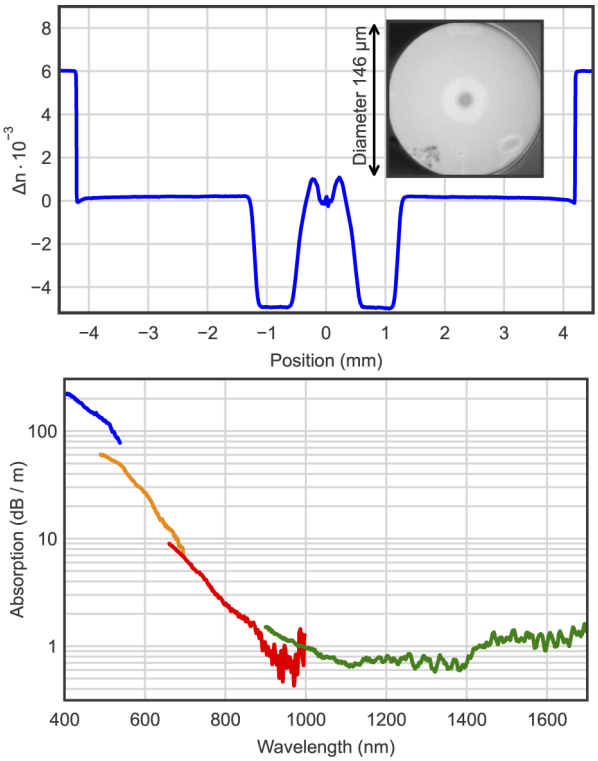

Fig. 1. Top: Refractive index profile of the Ce-doped preform. (Inset: cross-section of Ce-doped fiber.); Bottom: Absorption spectrum of Ce-doped fiber over the wavelength region of 400 to 1700 nm.

an Al Kα X-ray source and an Argus electron spectrometer (Omicron Nanotechnology GmbH). The core level spectra were collected with a pass energy of 20 eV, high magnification lens mode, and an in-lens aperture yielding circular analysis area of 3.14 mm^2 (Ø2.0 mm) The surface composition was identified by analyzing core level spectra using CasaXPS software (Version 2.3.19 PR 1.0). The binding energy scale was calibrated according to C 1s (C-C/H) at 284.8 eV. The surface composition of a preform fiber cross-section is presented in the Appendix B.

Figure 2 depicts the Ce 3d XPS spectrum which is adequately described with two pairs of peaks $d_{5/2}$ and $d_{3/2}$ spin-orbit coupled states. These peaks are then fitted using fixed line width and area ratio of 3:2 between the $d_{5/2}$ and $d_{3/2}$ components. The two douplet peaks, (v^0at 882.5 eV, u^0 at 900.9 eV) and (v' at 886.3 eV, u' at 904.8 eV), correspond to binary final states of Ce^{3+}, Ce $3d^94f^2$ - O $2p^5$ and Ce $3d^94f^1$ - O $2p^6$, respectively [19]. The $d_{3/2}$ level of Ce $3d^94f^0$ - O $2p^6$ final state at 918.5 eV (u''') is a fingerprint of Ce^{4+}. The low XPS intensity at 918.5 eV indicates that Ce is present primarily as Ce^{3+}.

Excitation-emission for the Ce-doped preform and fiber sample are measured using a FLS-1000 spectrofluorometer equipped with calibrated integrating sphere (Edinburgh Instruments, UK). A dwell time of 0.2 seconds and slit width of 5 nm is used for both excitation and emission measurements. The doped preform and the fiber sample is excited in the broad wavelength range of 350 nm to 750 nm with 20 nm step, and the emission spectra are recorded from 400 nm till 800 nm (1 nm increment), see Fig. 3(Top). For excitation wavelengths > 570 nm the observed luminescence is comparable to the noise level of the measurement system and hence is not depicted in Fig. 3. Each excitation wavelength results in a single emission band corresponding to

Optical Materials EXPRESS

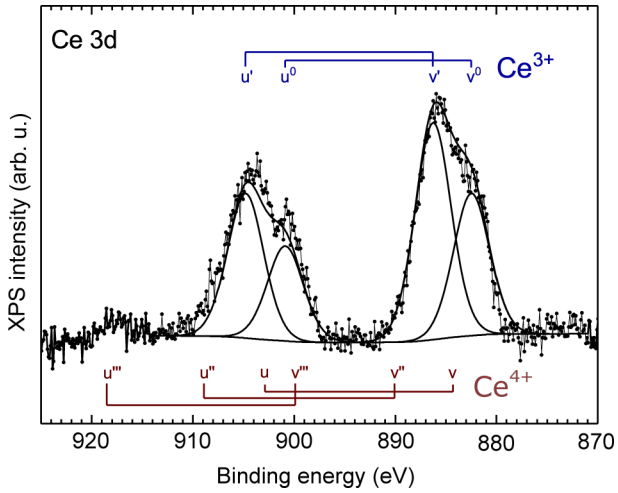

Fig. 2. Ce 3d XPS spectrum for Ce-doped preform cross-section. Distinct lineshape positions corresponding to different final states of Ce^{3+} (v0, v', u0, u') and Ce^{4+} (v, v'', v''', u, u'', u''') are marked in the figure.

single transition between energy levels of Ce^{3+} ion. The intensity of emission lines is a function of the excitation wavelength with the strongest emission obtained for excitation wavelength of 430 nm. A decrease in Stoke's shift from 101 nm to ~15 nm is observed with increasing excitation wavelength. The maximum shift between absorption and emission wavelengths is observed for the shortest excitation wavelength of 350 nm. For wavelengths longer than 570 nm Stokes shift stays relatively unchanged at ~15 nm. This indicates the energy transfer among the same energy levels for excited and emitted photons. When excitation wavelength is changed from 350 nm to 570 nm the emission peak wavelength shifts from 451 to 585 nm, which is quite a broad wavelength range for both excitation and emission wavelengths assuming a simple duplet energy level structure (as shown in the Dieke diagram) for Ce^{3+}-doped silicate glass [20,21]. This observation can be attributed to a strong splitting of the crystal-field, as exhibited by Ce^{3+} ions in fluoride glasses. This effect results in the red shift of the *5d* energy levels. Furthermore, it also affects the splitting of *4f* or *5d* states similar to Ce^{3+}-garnet crystal as described in [11,12].

The emission spectra of Ce-doped preform and fiber sample are nearly identical with small deviation at the excitation wavelengths of 350 ad 370 nm (Fig. 3(Bottom)). We attribute this to the waveguiding issue of a Ce-doped fiber.

2.3. Experimental setup

Figure 4 shows the schematic of the experimental setup used in this work to perform the spectral and output power measurements. The setup consists of a pump laser, the Ce-doped fiber, a multimode fiber, and a spectrometer. TO-Can packaged diode lasers are used as the pump source. Operating temperature of all lasers is kept constant at 20 °C using a TEC controller. The pump laser output is coupled into the Ce-doped fiber using an aspheric lens assembly. The other end of the Ce-fiber is butt-coupled to a multimode fiber with a core diameter of 600 µm (Ocean Optics QP-1-VIS-NIR). The fluorescence spectra are recorded with a Labsphere CDS-600 spectrometer. The spectrometer has a wavelength resolution of 2 nm and a scan range from 350 nm to 1100 nm.

To explore the quenching effect by multi-phonon, non-radiative relaxation and find the optimum energy transfer condition from the ground state to the upper excited states of Ce^{2+}-ions, several pump sources with wavelengths of 405 nm, 413 nm, 416 nm, 420 nm, and 440 nm are tested. After establishing the optimal pump wavelength the correlation between fiber length, pump power,

Optical Materials EXPRESS

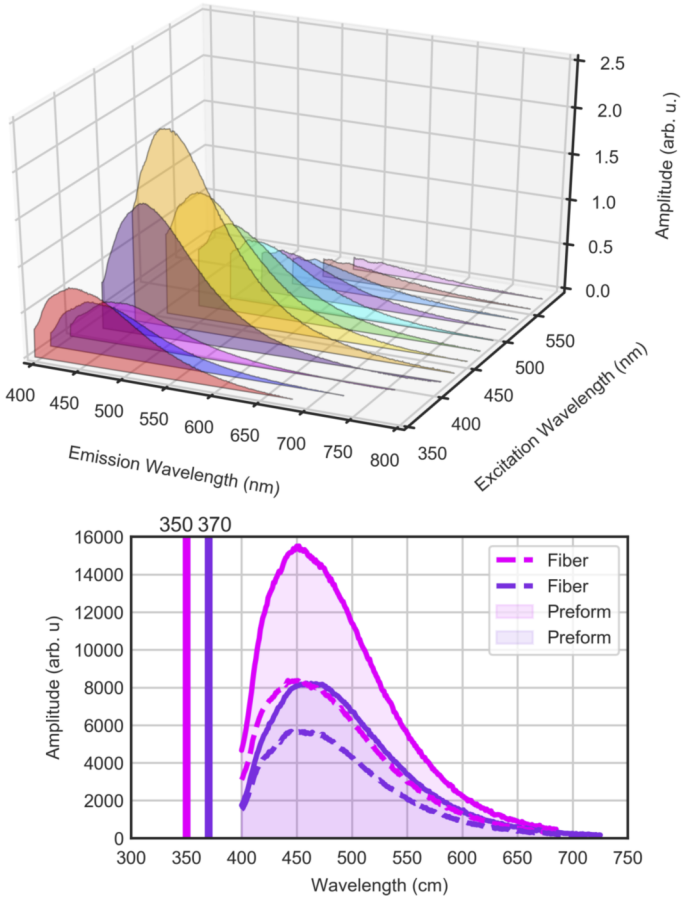

Fig. 3. Top: Excitation-Emission Map Measurements of Ce-doped preform; Bottom: The difference in emission spectra of Ce-doped preform and fiber sample under excitation at 350 nm and 370 nm.

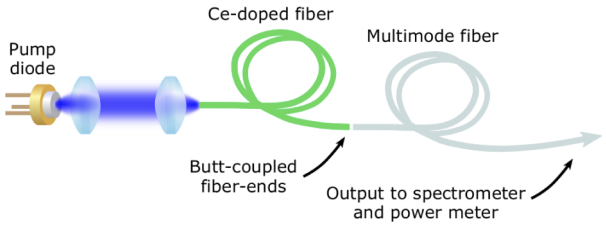

Fig. 4. Schematic for the experimental setup.

Optical Materials EXPRESS

and fluorescence output is investigated. Towards this, the fluorescence spectra and output powers are measured at different fiber lengths and pump powers. Starting with an initial Ce-doped fiber length of 170 cm, the fiber length is reduced in ~ 10 cm steps down to 30 cm. At each fiber length the fluorescence spectra and output powers are recorded for different pump powers. The input end of the Ce-doped fiber remains fixed throughout the experiment, preserving pump laser alignment and ensuring identical excitation conditions at different fiber lengths. The fiber is cut only from the output end, since the alignment of the multimode fiber is less sensitive.

3. Results and discussion

To study pump absorption of the Ce-doped fiber, we compare different pump wavelengths in the blue region of the optical spectrum between 405 nm and 440 nm. A 70 cm long fiber is pumped at different wavelengths with pump powers between 12 mW to 16 mW. Figure 5 depicts the measured fluorescence spectra for all tested pump wavelengths, except for the 440 nm pump wavelength at which only negligible fluorescence can be observed. The most efficient pump-to-signal power conversion is observed for the pump wavelength of 405 nm. This pump wavelength corresponds to the Ce^{3+}-ion transition from *4f* to the *5d* manifold. From the upper levels of *5d* manifold, the Ce^{3+}-ion radiatively relaxes by phonon-assisted processes to the lower levels of the same manifold. Afterwards, the Ce^{3+}-ion radiatively relaxes to the *4f* manifolds, emitting light in a broad spectral range from visible to NIR part of the optical spectrum. It could be worth to consider even shorter pump wavelengths to populate the *5d* manifold, however, further decrease of pump wavelength would lead to strong pump absorption in SiO_2 [22] resulting in decreased efficiency.

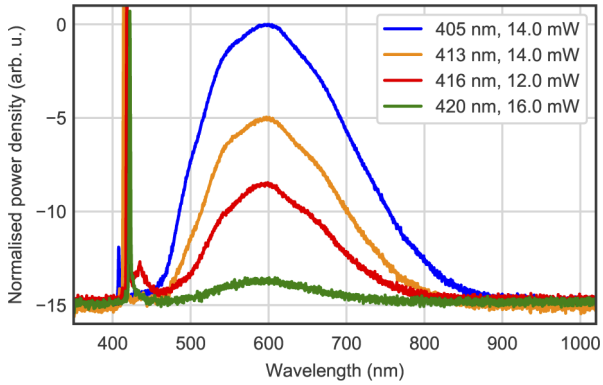

Fig. 5. Fluorescence Spectrum at different pump wavelengths.

After identifying the optimal pump wavelength of 405 nm, the influence of pump power and fiber length on the fluorescence output is investigated. Variation of pump power and fiber length is used to determine the optimal parameters for broadband fluorescence. We begin by measuring the fluorescence spectra and output powers for a 170 cm long fiber at discrete pump powers of 30 mW, 62.5 mW, 94.8 mW, and 127.4 mW. Fluorescence and output power measurements at the same pump powers are then repeated for different fiber lengths (see section 2.3). All measurements are performed at the pump wavelength of 405 nm. Unabsorbed pump light is observed only at fiber lengths shorter than 70 cm, while at longer fiber lengths the pump light is completely absorbed. The pump absorption is estimated from the measurement data to be ~ 2 dB/cm.

Figure 6 shows the estimated and measured fluorescence spectra for different fiber lengths respectively. Considering Ce upper level to be nearly empty due to short lifetime and large area of

Optical Materials EXPRESS

fiber core in the absence of any pump then for small pump powers (few mWs), due to high pump absorption(see fig.1 (bottom)) at 405 nm, we can consider nearly constant pump absorption along the fiber length. It would mean that nearly all (> 90%) pump power is absorbed along the first ~ 5cm of the fiber length and then we obtain nearly pure absorption of the emitted fluorescence by the Ce-doped fiber with absorption coefficients shown in fig. 1(bottom). This consideration can be used to estimate fluorescence spectra passed through a certain length of Ce-doped fiber. Fig. 6 (top) depicts measured initial fluorescence (for short piece < 10 mm of fiber without re-absorption) and estimated fluorescence for different fiber lengths.This is in good agreement with the measured fluorescence spectra for various fiber lengths up to 170 cm as shown in fig. 6 (bottom).

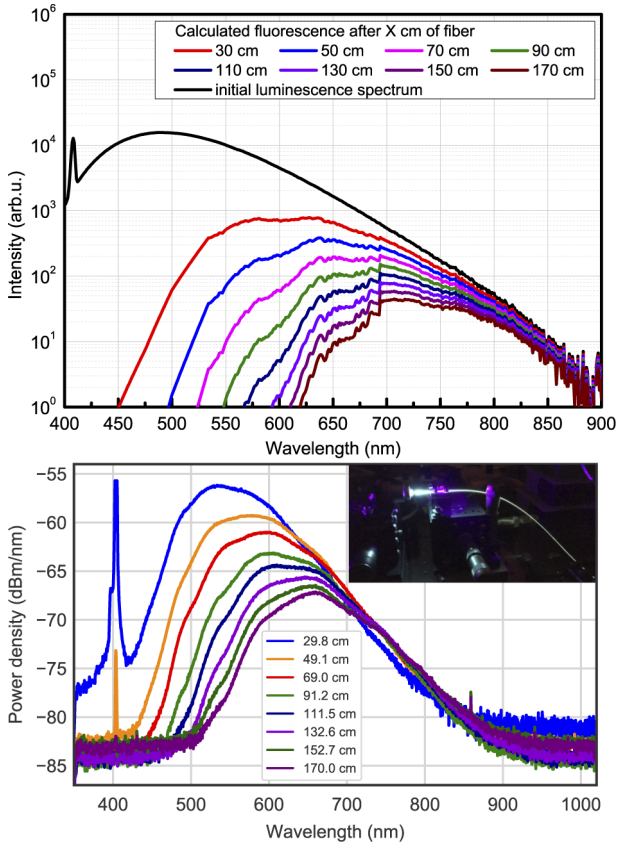

Fig. 6. Top: Measured fluorescence spectra of < 10 mm long fiber for ~ 405 nm pump and estimated spectra for different fiber lengths; Bottom: Fluorescence spectra at 127.4 mW pump power for different fiber lengths.

Figure 6 (bottom) depicts the measured fluorescence spectra for a pump power of 127.4 mW at different fiber lengths. The highest spectral power density of 2.4 nW/nm is observed at a wavelength of 533 nm for a fiber length of 30 cm. As the fiber length increases, the spectral power density in the short wavelength part of the spectrum (below ~ 650 nm) is strongly reduced. At the longest fiber length of 170 cm, the fluorescence is fully suppressed at wavelengths below ~ 500 nm. The suppression of the short wavelength part of the fluorescence results in a shift of peak wavelength with increasing fiber lengths. We suggest that this wavelength shift and spectral reshaping with fiber length is primarily due to re-absorption at Ce^{3+}-ion sites.

Optical Materials EXPRESS

Figure 7(a) shows the peak wavelength and wavelength range (at -10 dB) of the measured fluorescence for all investigated pump powers and fiber lengths. The peak wavelength shifts by ~120 nm from ~540 nm (at 30 cm) to ~660 nm (at 170 cm) and is almost independent of pump power. The measured fluorescence bandwidths (full-width at -10 dB) are presented in Fig. 7(b). At constant pump power, the fluorescence bandwidth increases with longer fiber lengths until a maximum is reached around 130 cm to 150 cm. Increase of pump power has no influence on fluorescence bandwidth at shorter fiber lengths and slightly reduces the obtained bandwidths at fiber lengths above 130 cm. For all measurements the bandwidth remains in the range of 230 nm to 301 nm. A bandwidth of ~280 nm is observed for fiber lengths of 133 cm and 142 cm at pump powers of 62.5 mW and 94.8 mW, with output optical powers of 20.5 nW and 18.3 nW, respectively. The maximum bandwidth of 301 nm is observed for the fiber length of ~133 cm at 30 mW pump power.

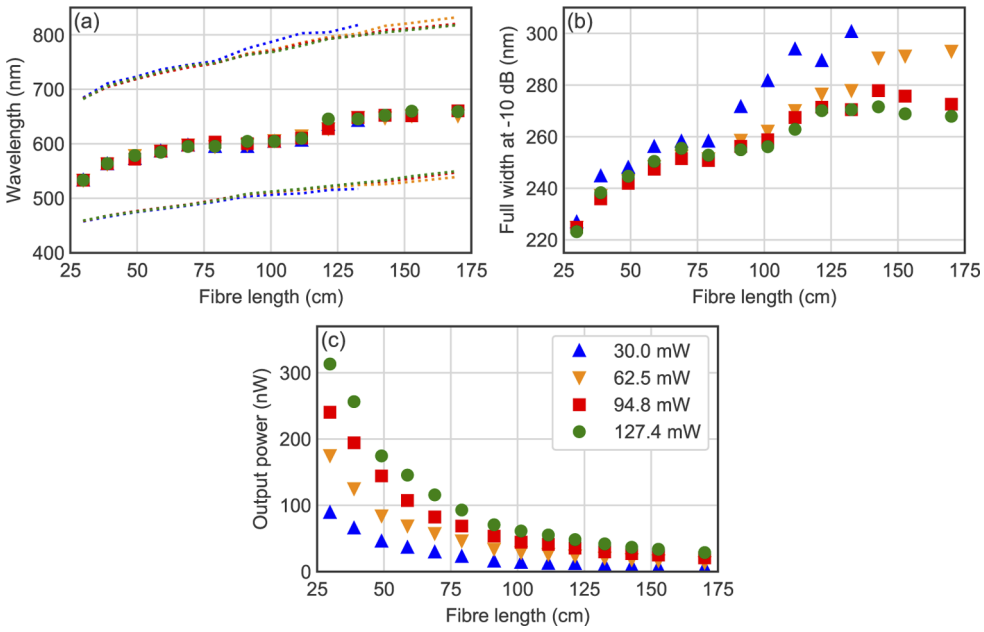

Fig. 7. Fluorescence characteristics as a function of fiber length and pump power at 405 nm: (a) peak wavelength (solid symbols) and wavelength range at -10 dB (dotted lines), (b) full-width at -10 dB, and (c) fluorescence output power.

The measured fluorescence output power (excluding the residual pump at shorter fiber lengths) as a function of fiber length at different pump powers is shown in Fig. 7(c). The output power gradually increases with decrease of the fiber length reaching the maximum value of 310 nW for a fiber length of 30 cm and a pump power of 127.4 mW. The increase in fluorescence power at shorter fiber lengths can be explained by reduced re-absorption in Ce-ions and smaller fiber propagation losses.

4. Summary

In summary, we demonstrate broadband, visible to NIR fluorescence from a Ce-doped silica fiber, with power densities of up to 2.4 nW/nm, using a 405 nm blue pump source. By variation of fiber length and pump power, we are able to obtain fluorescence in the wavelength range from 458 nm to 819 nm. We observe a shift of the fluorescence spectra to longer wavelengths with increasing fiber lengths, corresponding to a peak wavelength shift of ~120 nm from ~540 nm (at 30 cm) to

Optical Materials EXPRESS

~660 nm (at 170 cm). The broad spectrum was a result of direct energy transitions between the existing energy levels of Ce^{3+} ions. However, the fiber demonstrated a reabsorption of shorter wavelength emission with the increase of the fiber length leading to the emission spectrum shifting towards longer wavelength. Finally, by optimization of fiber length and pump power, we demonstrate a fluorescence bandwidth of 301 nm at -10 dB. To the best of our knowledge, this is the broadest fluorescence bandwidth demonstrated from Ce-doped fibers.

Appendix A .Experimental details on ICP-MS measurement

Trace metal analysis was performed by inductively coupled plasma mass spectrometry (ICP-MS) using Thermo Scientific iCAP RQ equipment. The instrument was equipped with a MicroMist borosilicate nebulizer 400 µl/min (Glass Expansion, Australia), a Peltier-cooled quartz spray chamber operating at 3 °C, a 2.5 mm ID quartz injector, a demountable quartz torch, a Ni skimmer cone and a high matrix interface skimmer cone insert. All measurements were performed in Kinetic Energy Discrimination (KED) mode using He as collision gas in the collision/reaction cell and Ar as the carrier gas. The instrument was tuned using a solution containing 1 µg/l of Ba, Bi, Ce, Co, In, Li and U for high sensitivity and minimum oxide levels (CeO/Ce < 2%). The measurement and analysis were performed using eQuant evaluation mode within Qtegra ISDS Software. Online addition of an internal standard solution containing 1 µg/l U, 1 µg/l Rh and 5 µg/l Ge in 2% HNO_3 (Romil-SpA) was used for the correction of nonspectral interferences in the analysis. Ionic standard solutions for analytes were prepared in 2% HNO_3 using ICP grade chemical containing all the rear earth elements (67349 Rare earth element mix for ICP, Sigma-Aldrich), and were applied to measure the calibration curves. Ultrapure H_2O (18.2 MΩ cm, Merck Milli-Q) and super pure acids (Romil-SpA) were used for all sample preparations.

For the ICP-MS measurement solid glass fiber was acid digested. First, a piece of Ce-doped glass fiber (m = 5.2 mg) was dissolved in 25 ml 2.5% HF at 63 °C. Complete dissolution resulted within 6 h. Then, HF was neutralized by addition of 0.1 g H_3BO_3 in the solution. Finally, 1 ml HNO_3 was added to the solution and solution was diluted to 50 ml with H_2O. Solution without glass fiber was prepared following the same processing stages and used as the blank sample. Measured values were normalized to the mass of the glass fiber.

Appendix B Experimental results (XPS)

The Ce-doped glass sample had two visually different concentric circular areas at the center with diameters of 2.5 mm and 1.0 mm (c.f. picture (Fig. 8) below). The XPS analysis was made at the center of the sample without any surface treatment. The sample was delivered inside tissue paper.

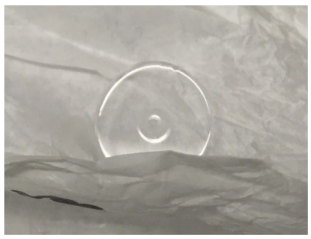

Fig. 8. Ce-doped glass sample.

XPS survey spectrum with identified elements on the surface is presented in Fig. 9. Table 2 depicts the elemental surface composition of Ce-doped glass sample). C, Na, Ca and Zn are impurities on the surface.

Optical Materials EXPRESS

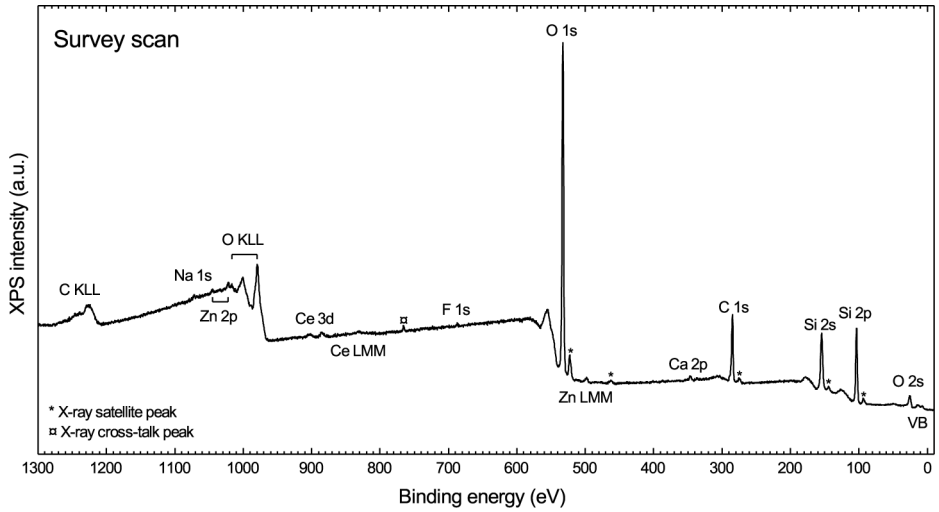

Fig. 9. XPS survey scan for Ce-doped glass sample.

Table 2. XPS-1 Surface composition of Ce-doped glass sample

at.%	O	C	Si	F	Ce	Na	Zn	Ca
Ce-doped glass	40.0	21.1	37.6	0.21	0.12	0.12	0.09	0.71

Funding. Engineering and Physical Sciences Research Council (EP/R024898/1); H2020 Marie Skłodowska-Curie Actions (843801); Jane & Aatos Erkko Foundation, Business Finland (1464/31/2019); Academy of Finland (326406, 326461); Ministry of Science and Higher Education of the Russian Federation (AAAA-A19- 119012590263-7, AAAA-A19-119011-690112-0, theme 0095-2019-006); Academy of Finland Flagship Programme, Photonics Research and Innovation (PREIN) (320165).

Acknowledgments. The authors thank Dr. Nikita Durandin (Tampere University) for providing of excitation-emission map measurements. This project has received funding from the European Union's Horizon 2020 research and innovation programme under the Marie Skłodowska-Curie Actions grant agreement No 843801. This work is part of the Academy of Finland Flagship Programme, Photonics Research and Innovation (PREIN) (decision No 320165). This work was supported by Jane & Aatos Erkko Foundation, Business Finland (decision No 1464/31/2019), Academy of Finland (grant Nos. 326461, 326406), and EPSRC (EP/R024898/1). This work was supported in part by the Russian Federation Ministry of Science and Higher Education (Project AAAA-A19-119011-690112-0 and AAAA-A19-119012590263-7, theme 0095-2019-006).

Disclosures. The authors declare no conflicts of interest.

Data availability. Data underlying the results presented in this paper are not publicly available at this time but may be obtained from the authors upon reasonable request.

References

1. W. Yen, M. Raukas, S. Basun, W. van Schaik, and U. Happek, "Optical and photoconductive properties of cerium-doped crystalline solids," J. Lumin. **69**(5-6), 287–294 (1996).
2. A. Vedda, N. Chiodini, D. Di Martino, M. Fasoli, S. Keffer, A. Lauria, M. Martini, F. Moretti, G. Spinolo, M. Nikl, N. Solovieva, and G. Brambilla, "Ce^{3+} -doped fibers for remote radiation dosimetry," Appl. Phys. Lett. **85**(26), 6356–6358 (2004).
3. R. Reisfeld, A. Patra, G. Panczer, and M. Gaft, "Spectroscopic properties of cerium in sol-gel glasses," Opt. Mater. **13**(1), 81–88 (1999).
4. X. Xu, K. Lebbou, F. Moretti, K. Pauwels, P. Lecoq, E. Auffray, and C. Dujardin, "Ce-doped LuAG single-crystal fibers grown from the melt for high-energy physics," Acta Mater. **67**, 232–238 (2014).
5. Q. Guo, X. Sun, W. Luo, J. Wen, F. Pang, C. Mou, G.-D. Peng, and T. Wang, "Scintillation and photoluminescence property of SiO_2 cladding YAP:Ce optical fiber via modified rod-in-tube method," Opt. Mater. Express **7**(5), 1525 (2017).
6. A. Herrmann, H. A. Othman, A. A. Assadi, M. Tiegel, S. Kuhn, and C. Rüssel, "Spectroscopic properties of cerium-doped aluminosilicate glasses," Opt. Mater. Express **5**(4), 720–732 (2015).

Optical Materials EXPRESS

7. M.-L. Brandily-Anne, J. Lumeau, L. Glebova, and L. B. Glebov, "Specific absorption spectra of cerium in multicomponent silicate glasses," J. Non-Cryst. Solids **356**(44-49), 2337–2343 (2010).
8. X. Sun, J. Wen, Q. Guo, F. Pang, Z. Chen, Y. Luo, G. Peng, and T. Wang, "Fluorescence properties and energy level structure of Ce-doped silica fiber materials," Opt. Mater. Express **7**(3), 751 (2017).
9. D. Coutts and A. McGonigle, "Cerium-doped fluoride lasers," IEEE J. Quantum Electron. **40**(10), 1430–1440 (2004).
10. A. Lapa, M. Cresswell, I. Campbell, P. Jackson, W. H. Goldmann, R. Detsch, and A. R. Boccaccini, "Gallium- and cerium-doped phosphate glasses with antibacterial properties for medical applications," Adv. Eng. Mater. **22**(9), 1901577 (2020).
11. J. Ueda and S. Tanabe, "(Invited) review of luminescent properties of Ce^{3+}-doped garnet phosphors: new insight into the effect of crystal and electronic structure," Opt. Mater.: X **1**, 100018 (2019).
12. C. Ma, F. Tang, J. Chen, R. Ma, X. Yuan, Z. Wen, J. Long, J. Li, M. Du, J. Zhang, and Y. Cao, "Spectral, energy resolution properties and green-yellow leds applications of transparent Ce^{3+}:$Lu_3Al_5O_12$ ceramics," J. Eur. Ceram. Soc. **36**(16), 4205–4213 (2016).
13. N. Chiodini, M. Fasoli, M. Martini, F. Morazzoni, E. Rosetta, R. Scotti, G. Spinolo, A. Vedda, M. Nikl, N. Solovieva, A. Baraldi, R. Capelletti, and R. Francini, "Rare-earth doped sol-gel silicate glasses for scintillator applications," Radiat. Eff. Defects Solids **158**(1-6), 463–467 (2003).
14. M. Alshourbagy, S. Bigotta, D. Herbert, A. D. Guerra, A. Toncelli, and M. Tonelli, "Optical and scintillation properties of Ce^{3+} doped $YAlO_3$ crystal fibers grown by μ-pulling down technique," J. Cryst. Growth **303**(2), 500–505 (2007).
15. Y. Hong, C. Jinlei, P. Yong, Z. Tiejun, and G. Shucai, "Photoluminescence properties of Tb^{3+} and Ce^{3+} co-doped $Sr_2MgSi_2O_7$ phosphors for solid-state lighting," J. Rare Earths **33**(4), 366–370 (2015).
16. C.-N. Liu, Y.-C. Huang, Y.-S. Lin, S.-Y. Wang, P.-L. Huang, T.-T. Shih, S.-L. Huang, and W.-H. Cheng, "Fabrication and characteristics of Ce-doped fiber for high-resolution OCT source," IEEE Photonics Technol. Lett. **26**(15), 1499–1502 (2014).
17. C.-N. Liu, Y.-C. Huang, P.-L. Huang, N.-K. Chen, C.-P. Yu, S.-L. Huang, and W.-H. Cheng, "Broadband Ce/Cr-doped crystal fibers for high axial resolution OCT light source," Opt. Express **23**(23), 29723 (2015).
18. V. F. Khopin, A. A. Umnikov, A. N. Gur'yanov, M. M. Bubnov, A. K. Senatorov, and E. M. Dianov, "Doping of optical fiber preforms via porous silica layer infiltration with salt solutions," Inorg. Mater. **41**(3), 303–307 (2005).
19. E. Bêche, P. Charvin, D. Perarnau, S. Abanades, and G. Flamant, "Ce 3D XPS investigation of cerium oxides and mixed cerium oxide ($Ce_xTi_yO_z$)," Surf. Interface Anal. **40**(3-4), 264–267 (2008).
20. C.-G. Ma, M. G. Brik, D.-X. Liu, B. Feng, Y. Tian, and A. Suchocki, "Energy level schemes of f^N electronic configurations for the di-, tri-, and tetravalent lanthanides and actinides in a free state," J. Lumin. **170**, 369–374 (2016).
21. M. J. Dejneka, A. Streltsov, S. Pal, A. G. Frutos, C. L. Powell, K. Yost, P. K. Yuen, U. Müller, and J. Lahiri, "Rare earth-doped glass microbarcodes," Proc. Natl. Acad. Sci. **100**(2), 389–393 (2003).
22. R. M. Atkins, "Measurement of the ultraviolet absorption spectrum of optical fibers," Opt. Lett. **17**(7), 469–471 (1992).